IOP Publishing Journal of Physics: Condensed Matter
J. Phys.: Condens. Matter **32** (2020) 285301 (10pp) https://doi.org/10.1088/1361-648X/ab7df4

Analytical study on strain tunable electronic structure and optical transitions in armchair black phosphorene nanoribbons

Pu Liu[1], Xiaoying Zhou[1,3], Xianbo Xiao[2], Benliang Zhou[1] and Guanghui Zhou[1,3]

[1] Department of Physics and Key Laboratory for Low-Dimensional Structures and Quantum Manipulation (Ministry of Education), Hunan Normal University, Changsha 410081, People's Republic of China
[2] School of Computer Science, Jiangxi University of Traditional Chinese Medicine, Nanchang 330004, People's Republic of China

E-mail: xiaoyingzhou@hunnu.edu.cn and ghzhou@hunnu.edu.cn

Received 14 November 2019, revised 21 February 2020
Accepted for publication 9 March 2020
Published 15 April 2020

Abstract

We theoretically investigate the electronic structure and optical absorption spectrum of armchair-edged black phosphorene nanoribbons (APNRs) with and without uniaxial strain based on the tight-binding Hamiltonian and Kubo formula. We analytically obtain the energy spectrum and wavefunction, and reveal the band gap scaling law as $1/(N+1)^2$ for APNRs in the presence and absence of uniaxial strain, where N is the number of armchair dimer across the ribbon. We find the band gap of APNRs linearly increases (decreases) with increasing in-plane uniaxial tensile (compressive) strain $\varepsilon_{x/y}$, but shows contrary dependence on the out-of-plane uniaxial strain ε_z. The effective mass versus strain exhibits the same behavior to that of band gap but with nonlinear dependence. Under an incident light linearly-polarized along the ribbon, we demonstrate that the inter-band optical transitions obey the selection rule $\Delta n = n - n' = 0$, but the intra-band transitions are forbidden for both pristine and strained APNRs originating from the orthogonality between the transverse wavefunctions of the sublattices belonging to different subbands. Importantly, the transverse electric field or impurities can release the optical selection rules by breaking the wavefunction orthogonality, which results in that the optical transitions between any subbands are all possible. Our findings provide further understanding on the electronic and optical properties of APNRs, which may pave the way for designing optoelectronic devices based on phosphorene.

Keywords: phosphorene nanoribbons, energy spectrum and wavefunction, uniaxial strain, optical transitions, tight-binding and Kubo formula

(Some figures may appear in colour only in the online journal)

1. Introduction

Two-dimensional (2D) black phosphorus (BP), as a promising candidate of future nanoelectronic components, has attracted intensive research attention [1–9] in recent years due to its unique electronic and optical properties. Unlike graphene, BP possesses a layer-dependent direct band gap ranging from 0.3 eV in the bulk to 1.8 eV in the monolayer [1, 10–12]. The field-effect-transistor (FET) based on monolayer BP (termed as phosphorene) exhibits an on/off ratio of 10^3 and a carrier mobility of 800 $cm^2\ V^{-1}\ s^{-1}$ [13]. Sizable band gap and relatively high mobility in phosphorene bridge the gap between graphene and monolayer transition metal dichalcogenides (TMDs), which are important for future nanodevices [8, 9, 12]. Inside phosphorene, phosphorus atoms are covalently bonded with three adjacent atoms to form a

[3] Authors to whom any correspondence should be addressed.

puckered honeycomb structure due to the sp^3 hybridization [11]. Arising from the low symmetric and high anisotropic structure, BP exhibits strongly anisotropic electrical [2, 14–17], optical [10, 12, 18, 19] and transport [20] properties.

Tailoring a 2D phosphorene into 1D nanoribbons provide a freedom to tune its electronic and optical properties arising from the quantum confinement and unique edge effects [19, 21–26]. Very recently, few-layer and monolayer BP nanoribbons are successfully synthesized in experiment [27–29]. The phosphorus atom configuration on the edge of phosphorene nanoribbons (PNRs) have two typical morphologic shapes, namely the armchair and zigzag. The armchair-edged PNRs (APNRs) are semiconductors with direct band gap depending on the number of armchair dimers N with scaling law of $1/(N+1)^2$ [19, 21, 25], while the bare zigzag-edged PNRs (ZPNRs) are always metallic due to the quasi-flat edge states [22, 23]. First principle and numerical tight-binding (TB) calculations have shown that the band structure of APNRs can be effectively modified by strain [26, 30], and external electric [23, 25, 31] or magnetic field [14]. Mechanically, phosphorene can hold up to 30% (27%) uniaxial tensile strain along the armchair (zigzag) direction predicted by the first-principle calculations [32]. Although there are already many research works on PNRs, the analytical calculation on the band structure of PNRs are rarely reported [22, 25, 33]. Most of the previous works are based on the first-principles calculation [19, 22, 26, 31] or numerical diagonalization utilizing the TB model [23, 25]. The analytical energy dispersion and wavefunction of ZPNRs based on TB model have been derived in our previous work [34]. For APNRs, the analytical forms of the energy spectrum and wave functions within the low energy regime have been worked out based on the low energy $k{\cdot}p$ Hamiltonian [25], which is qualitatively consistent with the TB calculations. A more accurate analytical calculations call for the TB method. Meanwhile, less attention has been paid to the optical property of APNR [21, 35], particularly the optical transition selection rule and the strain effect on them. However, optical spectrum measurements are fundamental approach to detect and understand the crystal band structure, which have been successfully performed for 2D phosphorene [12].

In this work, we theoretically study the electronic structure and optical absorption spectrum of APNRs in the presence and absence of uniaxial strain utilizing the TB Hamiltonian and Kubo formula. By solving the discrete Schordinger equation, in contrast to the method of numerical diagonalization on Hamiltonian, we analytically obtain the energy spectrum and wavefunction for APNRs with and without strain. Using the analytical result, we find that the band gap of APNRs scales as $1/(N+1)^2$ with N the number of armchair dimers across the ribbon, which was revealed previously by numerical TB [25] and first principle [19, 21] calculations. According to our results, this scaling law still holds even under uniaxial strain. Further, in the presence of uniaxial strain, we demonstrate that the band gap of a APNR increases (decreases) with increasing in-plane tensile (compressive) strain ($\varepsilon_{x/y}$), while the band gap dependence on the out-of-plane strain (ε_z) shows contrary behaviors to that of the in-plane one. The effective mass versus strain exhibits identical trend to that of band gap but with nonlinear dependence. For incident light linearly-polarized along the ribbon, the inter-band optical transitions obey the rule $\Delta n = n - n' = 0$, but the intra-band transitions are forbidden for both pristine and strained APNRs originating from the orthogonality between the wavefunctions of the A and B sublattices belonging to different subbands. The transverse electric field or impurities can release the optical selection rules by breaking the wavefunctions' orthogonality, leading to that the optical transitions between any subbands are all possible.

This paper is organized as follows. In section 2, we analytically calculate the band structure and the optical transition selection rule for $N-$APNR. In section 3, we present some examples and discussions on the band structure, effective mass and optical absorptions spectrum of APNRs. Finally, we summarize our results in section 4.

2. Electronic structure and optical selection rule for APNRs

2.1. Numerical diagonalization

In the top view of a typical N-APNR shown in figure 1(a), $\boldsymbol{a}_1$ and $\boldsymbol{a}_2$ are the primitive vector of 2D phosphorene with $a_1 = 4.38$ Å and $a_2 = 3.32$ Å , and $a = 2.207$ Å is the bond length between two adjacent atoms with bond angle $\alpha = 96.79^\circ$ [36]. There are four phosphorus atoms per unit cell with two in the lower layer and the other two in the upper one. Owing to the inversion symmetry [23], there are only two inequivalent atoms in the unit cell of 2D phosphorene sheet. We termed them as A and B in figure 1(a). The horizontal distance of two atoms in different sub-layers is $c = 0.706$ Å. The integers $1, 2, \ldots, N$ describe the number of dimer (two phosphorus sites) lines for APNRs, and the ribbon width is $(N-1)a_2/2$. The band structure of phosphorene can be well described by a five-parameter TB model [36, 37] shown in figure 1(a). In the presence of in-plane transverse electric field and impurities, the Hamiltonian of 2D phosphorene is given by

$$H = \sum_{\langle i,j\rangle} t_{ij} c_i^\dagger c_j + \sum_i (eE_t y_i + U_i) c_i^\dagger c_i, \tag{1}$$

where the summation $\langle i,j\rangle$ runs over all neighboring atomic sites with hopping integrals t_{ij}, and $c_i^\dagger$ (c_j) is the creation (annihilation) operator for atom site i (j). A transverse electric field E_t will shift the on-site energy to $eE_t y_i$ with y_i the atom coordination in the y-direction and U_i is the impurities potential. For pristine phosphorene, the five related hopping parameters [see figure 1(a)] are $t_1 = -1.22$ eV, $t_2 = 3.665$ eV, $t_3 = -0.205$ eV, $t_4 = -0.105$ eV, and $t_5 = -0.055$ eV [36]. For an N-APNR with the number of dimers N across the width, by applying the Bloch's theorem the TB Hamiltonian in the momentum space is [38]

$$H = H_{00} + H_{01} e^{ik_x a_1} + H_{01}^\dagger e^{-ik_x a_1}, \tag{2}$$

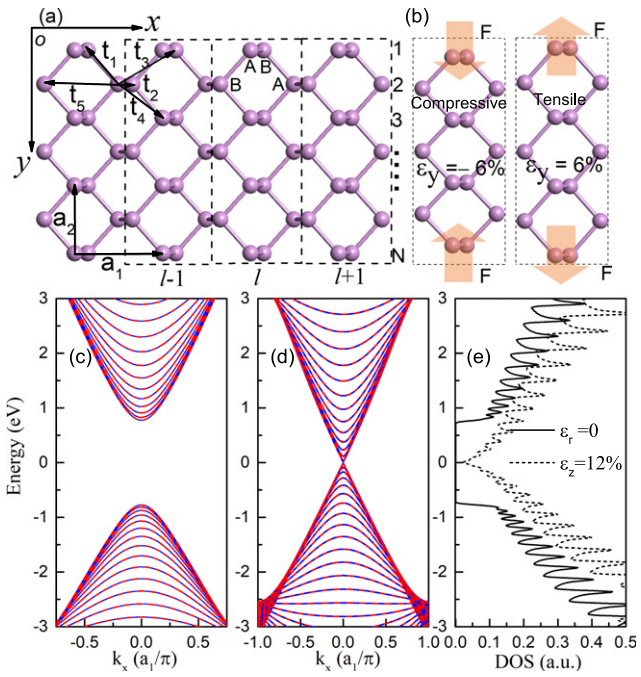

Figure 1. (a) Top view of a typical $N-$APNR with $|\boldsymbol{a}_1| = 4.38$ Å and $|\boldsymbol{a}_2| = 3.32$ Å. The bond length between two adjacent atoms is $a = 2.207$ Å with bond angle $\alpha = 96.79°$. (b) Sketch maps for a APNR under typical uniaxially tensile and compressive strain applied in the y-direction. The band structure of 30-APNR (c) without strain and (d) with uniaxial tensile strain $\varepsilon_z = 12\%$, where the (red) dashed lines represent the analytical subbands expressed in equation (11) and the (blue) solid lines indicate the numerical results based on the TB model. (e) Density of states corresponding to (c) and (d).

where H_{00} (H_{01}) describes the intra (inter)-supercell [see the (black) dashed-line rectangles in figure 1] interactions, k_x is the wavevector along the armchair direction. In our calculation, we accordingly choose the basis ordered as $(|1\mathrm{A}\rangle, |1\mathrm{B}\rangle, |2\mathrm{A}\rangle, |2\mathrm{B}\rangle, \ldots, |m\mathrm{A}\rangle, |m\mathrm{B}\rangle, \ldots, |N\mathrm{A}\rangle, |N\mathrm{B}\rangle)^{\mathrm{T}}$ to write done H_{00} and H_{01} in the form of $(2N \times 2N)$ matrix for the supercell adopted. Then, we can obtain the energy spectrum E_{n,k_x} and the corresponding wavefunction $|n, k_x\rangle$ for the system by numerical diagonalization.

On the other hand, strain is a powerful method to tune the electronic properties of phosphorene and its nanoribbons [26], and it is almost inevitable in fabricated monolayer nanostructures, manifesting as the formation of ridges and buckling. Figure 1(b) presents the schematics for a APNR under typical uniaxial compressive ($\varepsilon_y = -6\%$) and tensile ($\varepsilon_y = 6\%$) strain exerted along the y-direction. The arrows indicate the directions of the external forces which produce uniaxial strain. Uniaxial strains applied along the x- or z-direction are similar to that in the y-direction. For briefness, we use positive (negative) ε_{r} to denote the tensile (compressive) strain throughout the paper. Mechanically, phosphorene can hold up to 30% (27%) uniaxial tensile strain along the armchair (zigzag) direction predicted by first-principle calculations [32]. In our calculation, we only consider the strain within 15% in order to fulfill to the linear deformation condition. When the phosphorene subjected to uniaxial strain, the hopping parameters t_i will change. Considering a uniaxial strain $\varepsilon = \mathrm{diag}(\varepsilon_x, \varepsilon_y, \varepsilon_z)$, the deformed coordinates $r = (x, y, z)$ are related to the original ones $r_0 = (x_0, y_0, z_0)$ by the relation [39]: $(x, y, z) = ((1 + \varepsilon_x)x_0, (1 + \varepsilon_y)y_0, (1 + \varepsilon_z)z_0)$. In the linear deformed regime, expanding the norm of r to the first order of ε, the deformed r can be expressed as

$$r_i/r_0 = 1 + \alpha_i^x\varepsilon_x + \alpha_i^y\varepsilon_y + \alpha_i^z\varepsilon_z \tag{3}$$

where the coefficients are $\alpha_i^x = x_{i0}^2/r_0^2, \alpha_i^y = y_{i0}^2/r_0^2, \alpha_i^z = z_{i0}^2/r_0^2$. According to the Harisson rule [40, 41], the hopping parameters for p-orbital are related to the bond length as $t_i' \propto r_i^{-2}$ and the angular dependence can be described by the hopping integrals along the σ or π bonds. Though the changes in angles are almost noticeable, the modification of the hopping parameters is much smaller than the effect resulting from the bond lengths deformation. Hence, one can consider only the variation of the bond lengths in the hopping modulation. Then, the strain-dependent hopping energy in the linearly deformed regime is given by

$$t_i' = t_i(r_i/r_i^0)^{-2} \approx t_i[1 - 2(\alpha_i^x\varepsilon_x + \alpha_i^y\varepsilon_y + \alpha_i^z\varepsilon_z)]. \tag{4}$$

In order to obtain the band structure and corresponding wavefunction in the presence of uniaxial strain, we only need to replace the hopping parameters t_i in Hamiltonian (2) with t_i'.

2.2. Analytical calculation

In this subsection, we outline a solution of the eigenvalue problem for an N-APNR. Neglecting the influence of the perpendicular direction, we only need to consider two inequivalent atoms in the supercell [23, 42]. The electron wavefunction in a APNR can be written in the form

$$\psi = C_{\mathrm{A}}|\psi_{\mathrm{A}}\rangle + C_{\mathrm{B}}|\psi_{\mathrm{B}}\rangle, \tag{5}$$

where $\psi_{\mathrm{A/B}}$ and $C_{\mathrm{A/B}}$ are wavefunctions and combination coefficients corresponding to A/B sublattices, respectively. Based on the translational invariance, we choose the plane-wave basis along the $x-$direction [see figure 1(a)]. Within the TB framework, the wavefunctions at two sublattice sites can be written as

$$\begin{aligned} |\psi_A\rangle &= \frac{1}{N_A}\sum_{m=1}^{N} \mathrm{e}^{ik_x x_{mA}}\phi_{mA}|mA\rangle, \\ |\psi_B\rangle &= \frac{1}{N_B}\sum_{m=1}^{N} \mathrm{e}^{ik_x x_{mB}}\phi_{mB}|mB\rangle, \end{aligned} \tag{6}$$

where $\phi_{m\mathrm{A/B}}$ are the wave functions at the mth A/B sublattices in the $y-$direction and $N_{\mathrm{A/B}}$ are the normalized coefficients, respectively. $|m\mathrm{A}\rangle$ and $|m\mathrm{B}\rangle$ are the wave functions of the hybrid wannier orbit of phosphorous located at A and B sublattices [36], respectively. To solve $\phi_{m\mathrm{A}}$ and $\phi_{m\mathrm{B}}$, we employ the hard-wall boundary condition

$$\phi_{0\mathrm{A}} = \phi_{0\mathrm{B}} = 0, \ \phi_{N+1\mathrm{A}} = \phi_{N+1\mathrm{B}} = 0. \tag{7}$$

Choosing $\phi_{m\mathrm{A}} = \phi_{m\mathrm{B}} = \sin(pm)$ and substituting them into equation (7), we obtain

$$p = \frac{n\pi}{N+1} = n\theta, \tag{8}$$

where $n = 1, 2, 3, \ldots, N$ is the subband index, p is the discretized wave vector in the y-direction, and $\theta = \frac{\pi}{N+1}$. Applying the normalization condition $\langle\psi_A|\psi_A\rangle = \langle\psi_B|\psi_B\rangle = 1$, we have $N_A = N_B = \sqrt{\frac{N_x(N+1)}{2}}$, where N_x is the number of unit cells along the $x-$direction. For a perfect and uniform ribbon we just need to consider one super-cell, therefore, from here on we set $N_x = 1$. Then, the wavefunction ψ in equation (5) can be written as

$$\psi_{n,k_x} = \sum_{m=1}^{N} (C_A e^{ik_x x_{mA}} \phi^n_{mA}|mA\rangle \pm C_B e^{ik_x x_{mB}} \phi^n_{mB}|mB\rangle), \quad (9)$$

where $\phi^n_{mA} = \phi^n_{mA} = \sqrt{2/(N+1)} \sin\left(\frac{n\pi}{N+1} m\right)$ is the wavefunction along the y-direction in equation (6), and $\pm$ indicates the conduction/valence band.

By substituting equations (9) and (1) into the Schrodinger equation $H\psi = E\psi$, we can easily obtain the following matrix expression:

$$\begin{pmatrix} h_{11} & h_{12} \\ h_{21} & h_{22} \end{pmatrix} \begin{pmatrix} C_A \\ C_B \end{pmatrix} = E \begin{pmatrix} C_A \\ C_B \end{pmatrix}, \quad (10)$$

where $h_{11} = 4t'_4 \cos(k_x a_1/2)\cos(p)$, $h_{12} = 2\cos(p)(t'^{-ik_x d}_1 + t'^{ik_x(2c+d)}_3) + (t'^{-ik_x(2d+c)}_5 + t'^{ik_x c}_2)$ and $h_{21} = h^*_{12}$. Then, we immediately obtain the solution for the energy as

$$E_{n,k_x} = 4t'_4 \cos(k_x a_1/2)\cos p \pm |h_{12}|, \quad (11)$$

with the normal of h_{12} given by

$$\begin{aligned} |h_{12}| = [&4t'^2_1 \cos^2 p + t'^2_2 + 4t'^2_3 \cos^2 p + t'^2_5 \\ &+ 4t'_3 t'_5 \cos p \cos(3k_x a_1/2) + 2(4t'_1 t'_3 \cos^2 p + t'_2 t'_5) \\ &\times \cos(k_x a_1) + 4(t'_1 t'_5 + t'_1 t'_2 + t'_2 t'_3) \\ &\times \cos p \cos(k_x a_1/2)]^{1/2}. \end{aligned}$$

On the other hand, the Schrodinger equation $H\psi = E\psi$ also results in $C_B = \pm C_A e^{-i\varphi(k_x,p)}$, where $\varphi(k_x, p)$ is the argument of h_{21}. To fulfill the normalized condition $|C_A|^2 + |C_B|^2 = 1$, we choose $C_A = 1/\sqrt{2}$ and $C_B = \pm e^{-i\varphi(k_x,p)}/\sqrt{2}$ [43, 49]. Therefore, equation (9) is written as

$$\begin{aligned} \psi_{n,k_x} = \frac{1}{\sqrt{2}} \sum_{m=1}^{N} &(e^{ik_x x_{mA}} \phi^n_{mA}|mA\rangle \pm e^{-i\varphi(k_x,p)} \\ &\times e^{ik_x x_{mB}} \phi^n_{mB}|mB\rangle). \end{aligned} \quad (12)$$

Subsequently, the density of states (DOS) can be calculated accordingly

$$D(E) = \frac{1}{2\pi} \sum_n \int_{BZ} \delta(E - E_{n,k_x}) dk_x, \quad (13)$$

where the k_x integration runs over the first Brillouin zone (BZ). Meanwhile, the effective mass can also be calculated by using $m^* = (\partial^2 E/\hbar^2 \partial k_x^2)^{-1}$.

In the absence of strain, APNRs are always semiconductors. According to equation (11), the band gap is

$$E^N_g = 2|t_2 + t_5 + 2(t_1 + t_3)\cos\theta|. \quad (14)$$

In the 2D limit ($N \to \infty$, $\theta \to 0$), the band gap reduces to the bulk band gap $E^{2D}_g = 2|t_2 + t_5 + 2(t_1 + t_3)| = 1.52$ eV. For large N, we have $\cos\theta \approx 1 - \theta^2/2$, in this case, the band gap can be rewritten as

$$E^N_g = 2|t_2 + t_5 + 2(t_1 + t_3) - (t_1 + t_3)\pi^2/(N+1)^2|, \quad (15)$$

which shows a $1/(N+1)^2$ band gap scaling law for APNRs recovered in previous work reported by first principle [19] and numerical TB calculations [25]. In the presence of uniaxial strain within the linear deformation regime, we just need to replace the hopping parameters expressed in equation (15) to obtain the band gap as

$$\begin{aligned} E^N_g(\varepsilon_r) = 2\big|E^N_g(0) - 2\varepsilon_r[&t_2\alpha^r_2 + t_5\alpha^r_5 \\ &+ 2(t_1\alpha^r_1 + t_3\alpha^r_3)\cos\theta]\big|, \end{aligned} \quad (16)$$

where $\varepsilon_r (r = x, y, z)$ is the tensile (compressive) uniaxial strain applied along the r direction. Equation (16) shows that the $1/(N+1)^2$ band gap scaling law of APNRs still holds even in the presence of uniaxial strain. It also indicates that the band gap of APNRs linearly depend on the uniaxial (tensile or compressive) strain along the r direction.

The band structures of 30-APNR without and with uniaxial tensile strain $\varepsilon_z = 12\%$ are presented in figures 1(c) and (d), respectively. As shown in the figures, our energy spectra analytically obtained from equation (11) [see the (red) dashed lines] perfectly matches the numerical TB dispersions [the (blue) solid lines] in both cases. In comparison figure 1(c) with figure 1(d), it indicates that the uniaxial strain effectively modifies the band structure of APNR. Under a 12% uniaxial tensile strain along the z-direction which may be realized experimentally by creating nanobubbles as that in graphene [44], the band gap is closed, leading to a semiconductor–metal transition with Dirac dispersion, which is consistent with the results in previous work [45]. The semiconductor–metal transition is also reflected in the density of states (DOS) depicted in figure 1(e). In the absence of strain, the DOS is zero near the Fermi energy. In contrast, there is a finite DOS near the Fermi level under the critical uniaxial strain along the z-direction. In addition, the number of peaks and the shape of the DOS in figure 1(e) reflect the main features of the band structure shown in figures 1(c) and (d). There are a sequence of sharp peaks in the DOS outside the band gap, which correspond to Van Hove singularities [46] induced by the extreme of their quantized subbands.

3. Optical selection rule

In order to detect the above calculated band structure of APNR, next we explore its optical response in this subsection. One useful physical quantity to understand the optical property is the joint density of states (JDOS) representing all possible optical transitions among the subbands, which is generally given by

$$D_J(\omega) = \frac{g_s}{L_x} \sum_{n,n',k_x} [f(E_{n,k_x}) - f(E_{n',k_x})]\delta(E_{n,k_x} - E_{n',k_x} + \hbar\omega), \quad (17)$$

where the sum runs over all states $|n,k_x\rangle$ and $|n',k_x\rangle$, g_s is 2 for spin degree, L_x the ribbon length, $\hbar\omega$ the photon energy, and $f(E) = 1/[\exp(E-E_F)/k_BT+1]$ the Fermi–Dirac distribution function with Boltzman constant k_B and temperature T. Here, we take a Lorenz broadening $\frac{1}{\pi}\frac{\Gamma}{(E_{n,k_x}-E_{n',k_x}+\hbar\omega)^2+\Gamma^2}$ to approximate the δ-function, where Γ is a phenomenological constant accounting for the energy level broadening factor. Meanwhile, assuming the incident light is polarized along the longitudinal (x-)direction, the optical conductance based on the Kubo formula is given by [47, 48]

$$\sigma(\omega) = \frac{g_s\hbar e^2}{iL_x}\sum_{n,n',k_x}\frac{[f(E_{n,k_x})-f(E_{n',k_x})]|\langle n,k_x|v_x|n',k_x\rangle|^2}{(E_{n,k_x}-E_{n',k_x})(E_{n,k_x}-E_{n',k_x}+\hbar\omega+i\Gamma)}, \tag{18}$$

where $v_x = \partial H/\partial p_x$ is the velocity operator, which is valid and independent of the band structure model, and $|n,k_x\rangle = \psi_{n,k_x}$ is the electron wavefunction in a APNR. For a linear polarized light, the optical transition matrix elements satisfy $v_{n,n'}(k_x) = \langle n,k_x|v_x|n',k_x\rangle = \langle\psi_{n,k_x}|v_x|\psi_{n',k_x}\rangle$, which determines the optical transition selection rules. A zero matrix element $v_{n,n'}(k_x)$ means a forbidden transition. The integral of the inter-band optical transition matrix elements $V_{n,n'} = \int \mathrm{d}k_x|v_{n,n'}(k_x)|^2$ is proportional to the transition probability between the nth and n'th subband.

By using the commutator $v_x = \frac{i}{\hbar}[x,H]$ combined with some arithmetic (see details in appendix), the optical transition matrix elements are obtained as

$$\langle n,k_x|\,v_x\,|n',k_x\rangle = \frac{i}{2\hbar}\sum_{m=1}^{N}[G_{n,n'}(1-\mathrm{e}^{\mathrm{i}[\varphi(k_x,p_n)-\varphi(k_x,p_{n'})]}) + F_{n,n'}\mathrm{e}^{-\mathrm{i}\varphi(k_x,p_{n'})}+F^*_{n,n'}\mathrm{e}^{\mathrm{i}\varphi(k_x,p_n)}]K_{n,n'}, \tag{19}$$

where $G_{n,n'} = 4it'_4\cos(n'\theta)(c+d)\sin[k_x(c+d)]$, $F_{n,n'} = 2\cos(n'\theta)[t'^{-\mathrm{i}k_xd}_1 - t'^{\mathrm{i}k_x(2c+d)}_3] + [(2d+c)t'^{-\mathrm{i}k_x(2d+c)}_5 - ct'^{\mathrm{i}k_xc}_2]$, and the overlap integral $K_{n,n'}$ between the wavefunction of A and B atoms corresponding to different subbands is given by

$$K_{n,n'} = \sum_{m=1}^{N}\phi^n_{m\mathrm{A}}\phi^{n'}_{m\mathrm{B}} = \delta_{n,n'}. \tag{20}$$

From equation (20), we find explicitly that the inter-band optical selection rule for APNR is $\Delta n = n-n' = 0$ regardless of the ribbon width, while the intra-band optical transitions are forbidden due to the orthogonality of the wavefunction corresponding to different sublattice i.e., the A and B atoms indicated in figure 1(a). In the presence of impurities or transverse electric field, the wavefunction in the $y-$direction does not have a simple sine form as expressed in equation (9). The overlap integration $K_{n,n'}$ will be a little bit complicated (see the appendix) and the orthogonality between the wavefunction of A and B sublattices belonging to different subbands will break down, leading to an enhanced optical absorption as shall be discussed later.

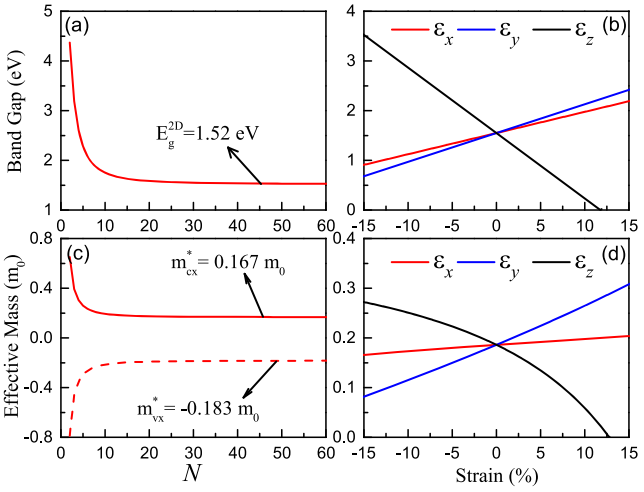

Figure 2. The band gap of APNRs as a function of (a) the number of dimers N and (b) uniaxial strain for $N = 30$. The effective masses of APNRs around CBM versus (c) the number of dimers N and (d) uniaxial strain for $N = 30$. The arrows in (a) and (b) represent the counterpart in 2D phosphorene. The red, blue and black lines in (b) and (d) indicates the uniaxial strain along the $x-$, $y-$ and $z-$direction, respectively.

4. Results and discussions

In this section, we will show some examples for the band structure and optical absorption spectra both with and without strain. The temperature is 4 K and the level broadening Γ is 4 meV here. In our work, we choose 30-APNR as a representative, and the Fermi level is 0 eV throughout the paper.

Figures 2(a) and (b) present the band gap of APNRs versus the number of dimers N and uniaxial strain with $N = 30$, respectively. As shown in figure 2(a), the band gap of pristine APNRs sensitively depend on the number of dimers N due to the quantum confinement [19, 23]. As expressed in equation (14), the band gap decreases rapidly to that of the 2D phosphorene sheet $E_g^{2D} = 1.52$ eV scaling as $1/(N+1)^2$, which is the same as that reported by the previous first principle [19] and numerical TB [25] calculations. According to figure 2(b), the APNR's band gap linearly increases (decreases) with increasing in plane uniaxial tensile (compressive) strain $\varepsilon_{x/y}$ (see the red and blue lines) with different slope. In contrast, it linearly decreases (increases) with the increasing of out-of plane uniaxial tensile (compressive) strain ε_z (see the black line). In principle, the both in-plane and out-of plane strains can close the band gap and induce a semiconductor–metal transition, but the critical in-plane strain is too large to realize experimentally. In our calculation, the critical strains closing the band gap along z-directions is $\varepsilon_z = 12\%$ tensile strain, which may be realized experimentally by creating nanobubbles as that in graphene [44]. At the critical value $\varepsilon_z = 12\%$, there is a Dirac dispersion as shown in figure 1(c), leading to a semiconductor–metal transition. Similarly, the effective masses around the CBM and VBM versus the the number of dimers are depicted in figure 2(c). As shown in the figure, both the effective masses around the CBM and

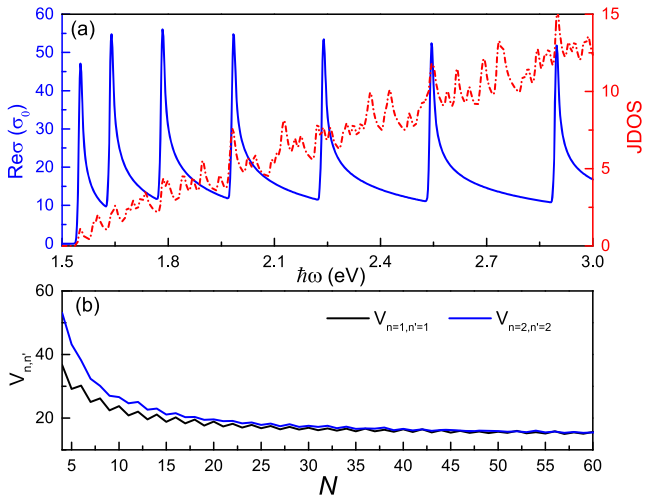

Figure 3. (a) The inter-band JDOS [(red) dashed-dotted lines] and the optical absorption [(blue) solid lines] as a function of incident photon energy with $\sigma_0 = 2e^2/h$ for 30-APNR. The Fermi level E_F is chosen as 0 eV. (b) The integral of the inter-band optical transition matrix elements $V_{n,n'} = \int dk_x |v_{n,n'}(k_x)|^2$ as a function of the ribbon width N.

VBM rapidly reduce to the counterpart of 2D phosphorene sheet [14] $m^*_{cx} = 0.167m_0, m^*_{vx} = 0.183m_0$ with increasing ribbon width. The effective mass around the CBM for 30-APNR versus uniaxial strain is presented in figure 2(d). As shown in the figure, we find the effective mass around CBM non-linearly depend on not only the out-of-plane component of the strain but also the in-plane strain because the dispersion is non-linearly dependent on the strain [see equation (11)]. In specification, the effective mass non-linearly increases with the increase of in-plane uniaxial strain $\varepsilon_{x/y}$ but decreases with the increase of out-of plane uniaxial strain ε_z. At the critical strain i.e., $\varepsilon_z = 12\%$, which closes the band gap, the effective mass becomes zero. The effective mass around the VBM versus uniaxial strain is not discussed here because there is little difference from that around CBM for a certain APNR.

Figure 3(a) presents the inter-band JDOS and the optical absorption as a function of incident photon energy for pristine 30-APNR. As shown by the (red) dashed line, we find JDOS peaks at different photon energy known as van Hove singularities, which present all possible optical transitions among subbands. Since pristine APNRs are always semiconductor, the JDOS peaks appear only when the photon energy is higher than the band gap. As disscussed in the section 3, in pristine or uniaxial strained APNRs, the interband optical selection rule is $\Delta n = n - n' = 0$ arising from the orthogonality between the wavefunctions of the A and B sublattice belonging to different subbands [see equation (20)]. This is explicitly reflected in the optical absorption spectrum. Compared the optical absorption spectrum with the JDOS one, we find that many absorption peaks are missing and only the absorption peaks satisfying the selection rule $\Delta n = 0$ appear, which is similar to that in gapped armchair graphene nanoribbons [49, 50]. Moreover, it should be noted that there is a little discrepancy between the JDOS and the optical absorption spectrum since the optical transition matrix element $\langle n, k_x | v_x | n', k_x \rangle$ sensitively depends on the derivatives $\partial E/\partial \hbar k_x$ of each subbands. The intra-band optical absorption are not discussed here because all intra-band transitions are forbidden according to equation (20). Figure 3(b) shows the integral of the interband velocity matrix element $V_{n,n'}$ which is proportional to the optical transition probability between the nth and n'th subbands as a function of the number of armchair dimer N, where the blue/black solid line indicates $V_{1,1}/V_{2,2}$. Here, we only need to consider the $n = n'$ case due to the optical transition rules in equation (20). As shown in the figure, we find both $V_{1,1}$ and $V_{2,2}$ gradually decrease to a identical value with the increasing of the ribbon width ($\sim N$). From equation (19), we know the $V_{n,n}$ was related to the ribbon width by $\cos^2(\theta n)$. For wider APNRs, we have $\theta \to 0$ and $\cos(\theta n) \to 1$, which means all of the allowed transition integrals trend to a identical value which are just the transition integrals of 2D phosphorene. If the light polarized perpendicularly to the ribbon axis, i.e., the zigzag (y-)direction, the optical transition selection rules will be different from the results reported here arising from the anisotropic optical absorption in 2D phosphorene [18]. Meanwhile, the corresponding optical conductance is smaller than the results discussed in this work because the effective mass along the zigzag direction is larger than that along the armchair direction.

Figure 4 presents the contour plot of the interband optical absorption conductance versus photon energy and uniaxial strain for 30-APNR. According to equation (19) or (20), the optical selection rule $\Delta n = 0$ still holds in the presence of uniaxial strain. Hence, we find only several conductance peaks in the absorption spectra and the resonance photon energy increased rapidly [see figures 4(a)–(c)] under a certain uniaxial strain. The photon energy of the band-edge absorption (BEA), namely the energy of the first absorption peak, which is just the band gap of APNRs under uniaxial strain, namely $E^N_g(\varepsilon_r)$. As shown in the figure, the energies of BEA are blue (red) shifted with increasing in-plane uniaxial tensile (compressive) strain $\varepsilon_{x/y}$ [see figures 4(a) and (b)], while it is red (blue) shifted with increasing out-of plane uniaxial tensile (compressive) strain ε_z [see figure 4(c)]. These mean that the energy of BEA can be used to determine the strain tunable band gap $E^N_g(\varepsilon_r)$ in equation (16). Compared with the unstrained data in figure 3(a), there are quantitative difference between them since the uniaxial strain modifies the effective masses significantly [see figure 2(d)]. Therefore, although the uniaxial strain does not change optical selection rule of APNRs, it modulates the optical absorption effectively by changing the band gap and effective masses.

A transverse electric field (TEF) can induce a Stark effect [51–53] for APNR which makes a significant change of the band structure and wavefunctions. Figure 5(a) depicts the inter-band JDOS [(red) dash-dotted line] and optical absorption [(blue) solid line] spectrum for 30-APNR under a TEF $E_t = 0.00$ eV Å^{-1} with corresponding band structure shown in figure 5(b). In the presence of TEF, the wavefunctions $\phi^n_{m\mathrm{A}}$ and $\phi^n_{m\mathrm{B}}$ are no longer the simple sine function described in

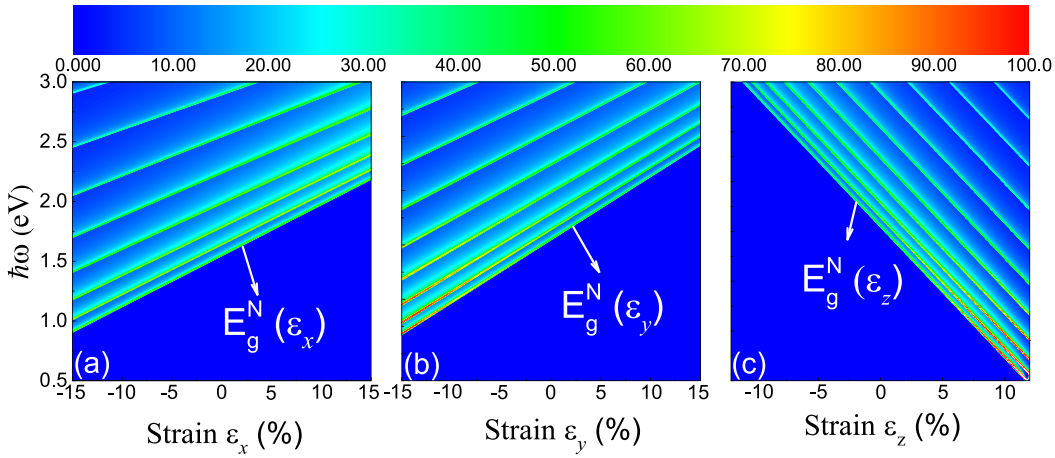

Figure 4. The inter-band optical absorption conductance in unit of $\sigma_0 = 2e^2/h$ as a function of the incident photon energy $\hbar\omega$ and uniaxial strain along the (a) $x-$, (b) $y-$ and (c) $z-$direction for 30-APNR. The arrows indicate the band gap versus uniaxial strained for 30-APNR.

equation (9), which will break the orthogonality relation in equation (20) (see the appendix). Therefore, the optical transitions are all possible between any different subbands. Indeed, compared the optical absorption data with that of pristine 30-APNR [see figure 3(a)], all missed optical absorption peaks reappear one to one correspondence to the JDOS due to the break down of the selection rule $\Delta n = 0$ arising from the invalidation of the orthogonality between the wavefuncions in the transverse direction. A stronger TEF can close the band gap and lead to the inversion of conduction and valence bands [52, 53] [see figure 5(d)]. Again, a TEF will release the optical selection rules regardless of its strength because it breaks the wavefunction orthogonality, which results in that the optical transitions between any subbands are all possible. Therefore, most of the optical absorption peaks are reappeared corresponding one to one with the JDOS shown in figure 5(c). However, many of the optical conductance peaks in the low frequency regime ($\hbar\omega < 1$ eV) are still missing. The reason is that the Stark effect induced by the TEF will reduce the overlap integral between the wavefunctions of the electron and hole state s [53], which influences the optical transition selection rules directly [see equation (A3)]. Therefore, in the band inversion regime, the optical transitions between the subbands with zero overlap integral are forbidden. This mainly happens in the low frequency regime since the wavefunction of the electron and hole states in the low energy regime are spatially separated [53]. Hence, the optical conductance in figure 5(c) in the low frequency regime is quite small [see the (blue) solid line].

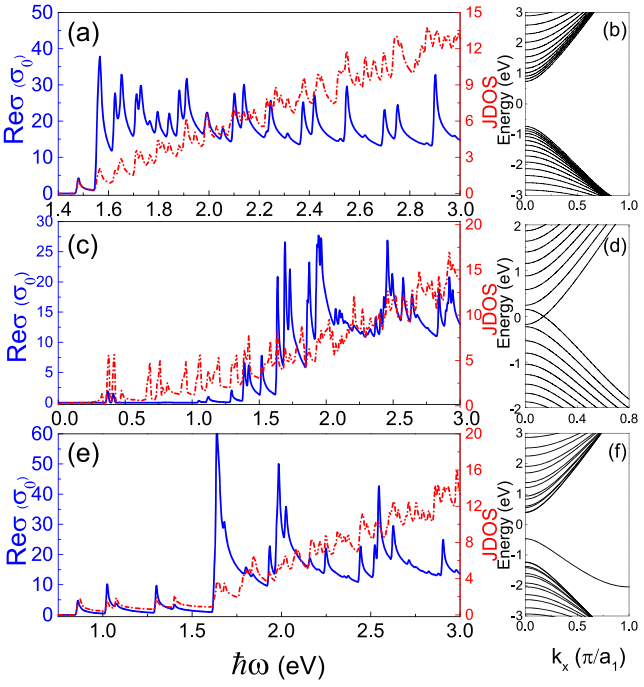

Figure 5. The inter-band JDOS [(red) dashed-dotted lines] and the optical absorption [(blue) solid lines] for 30-APNR under a uniform transverse electric field (a) 0.005 eV Å^{-1}, (c) $E_t = 0.057$ eV Å^{-1} and (e) with impurities localized at the ribbon center (the 15th row) with impurities potential $U_i = 2$ eV. The corresponding band structure of (a), (c) and (e) are shown in (b), (d) and (f), respectively.

In real experiment, it is difficult to avoid impurities and defects in samples, which may consequently affect the optical properties of APNRs by changing the band structure and wavefunction. Figure 5(e) presents the JDOS and optical absorption peaks for 30-APNR with impurities distribution on the ribbon center (the 15th dimer line). We model the impurity effect by changing the on-site energy of the corresponding atoms, which is widely used in previous works [54]. The impurities potential U_i equals to 2 eV and the corresponding band structure is shown in figure 5(f). From figure 5(f), we find the subbands contributed by the impurities are shifted but other subbands remain unchanged. However the impurities change the wavefunction of the APNRs and hence forth the optical transition selection rule. As shown in figure 5(e), we find some extra peaks in the optical absorption spectrum compared with that of the pristine 30-APNR. The reason is that the

wavefunctions of APNRs along the transverse direction in the presence of impurities are no longer the sine function expressed in equation (9). Hence, the orthogonality between the transverse wavefunction of the pristine APNRs, namely equation (20) become invalid (see the appendix), contributing to that the optical transitions among all subbands are possible. As a result, all the optical absorption peaks appear one to one correspondence to JDOS, which consequently enhances the optical absorption.

5. Summary

In summary, we have analytically studied the uniaxial strain effect on the electronic structure and optical absorption properties of APNRs utilizing the TB Hamiltonian and Kubo formula. We obtained the energy spectrum of APNRs under uniaxial strain analytically and reveal the $1/(N+1)^2$ band gap scaling law directly. In the presence of uniaxial strain, we find the band gap of a APNRs increases (decreases) with increasing tensile (compressive) in-plane uniaxial strain $\varepsilon_{x/y}$, while the band gap dependence on the out-of-plane uniaxial strain ε_z shows contrary behavior to that of the in-plane one. The effective mass versus strain exhibits the same trend as that of the band gap but with nonlinear dependence. Under an incident light linearly-polarized along the ribbon, we found that the inter-band optical selection rule is $\Delta n = n - n' = 0$, but the intra-band optical transitions are forbidden for both pristine and strained APNRs originating from the orthogonality between the wavefunctions of the A and B sublattice belonging to different subbands. Both the transverse electric fields and impurities can break the wavefunctions' orthogonality, and release the optical selection rules. Our results shed light on the optical transitions of APNRs, which may be useful in designing optoelectronic devices based on phosphorene.

Acknowledgments

This work was supported by the National Natural Science Foundation of China (Grant Nos. 11804092, 11774085, 11664019, and 11704118), and Project funded by China Postdoctoral Science Foundation (Grant Nos. BX20180097, 2019M652777), and Hunan Provincial Natural Science Foundation of China (Grant No. 2019JJ40187).

Appendix

To present the optical transition selection rule, we calculate the optical transition matrix element in equation (19). Utilizing the commutator $v_x = \frac{i}{\hbar}[x, H]$ [55] combined the general wavefunction equation (12)

$$\psi_{n,k_x} = \frac{1}{\sqrt{2}}\sum_{m=1}^{N}\left(\mathrm{e}^{\mathrm{i}k_x x_{m\mathrm{A}}}\phi^n_{m\mathrm{A}}|m\mathrm{A}\rangle \pm \mathrm{e}^{-\mathrm{i}\varphi(k_x,p)} \times \mathrm{e}^{\mathrm{i}k_x x_{m\mathrm{B}}}\phi^n_{m\mathrm{B}}|m\mathrm{B}\rangle\right), \tag{A1}$$

then the optical transition matrix elements for inter-band transition are obtained as

$$v_{n,n'}(k_x) = \langle n, k_x|\, v_x\, |n', k_x\rangle = \frac{i}{\hbar}\langle\psi_{n,k_x}|\, Hx - xH\, |\psi_{n',k_x}\rangle\,. \tag{A2}$$

There are four kinds of transitions, namely from A to A atoms, from B to B atoms, from A to B atoms and from B to A atoms. For the TB model of APNRs, there are also five hoppings between the different atoms, including $\langle m\mathrm{A}|\, H\, |m'\mathrm{B}\rangle = \langle m\mathrm{B}|\, H\, |m'\mathrm{A}\rangle = t'_1$ for $m' = m \pm 1$, $\langle m\mathrm{A}|\, H\, |m'\mathrm{B}\rangle = \langle m\mathrm{B}|\, H\, |m'\mathrm{A}\rangle = t'_2$ for $m' = m$, $\langle m\mathrm{A}|\, H\, |m'\mathrm{B}\rangle = \langle m\mathrm{B}|\, H\, |m'\mathrm{A}\rangle = t'_3$ for $m' = m \pm 1$, $\langle m\mathrm{A}|\, H\, |m'\mathrm{B}\rangle = \langle m\mathrm{B}|\, H\, |m'A\rangle = t'_4$ for $m' = m \pm 1$, and $\langle m\mathrm{A}|\, H\, |m'\mathrm{B}\rangle = \langle m\mathrm{B}|\, H\, |m'\mathrm{A}\rangle = t'_5$ for $m' = m$. Then, the transition matrix elements can be written as

$$\begin{aligned}
v_{n,n'}(k_x) = \frac{i}{2\hbar}\sum_{m,m'=1}^{N} & (x_{m'A} - x_{mA})\mathrm{e}^{ik_x(x_{m'A}-x_{mA})}(\phi^n_{mA})^*\phi^{n'}_{m'A}\langle mA|\, H\, |m'A\rangle - (x_{m'B} - x_{mA})\mathrm{e}^{ik_x(x_{m'B}-x_{mA})}\mathrm{e}^{-i\varphi(k_x,p_{n'})}(\phi^n_{mA})^* \\
& \times \phi^{n'}_{m'B}\langle mA|\, H\, |m'B\rangle - \mathrm{e}^{i[\varphi(k_x,p_n)-\varphi(k_x,p_{n'})]}(x_{m'B} - x_{mB})\mathrm{e}^{ik_x(x_{m'B}-x_{mB})}(\phi^n_{mB})^*\phi^{n'}_{m'B}\langle mB|\, H\, |m'B\rangle \\
& + (x_{m'A} - x_{mB})\mathrm{e}^{ik_x(x_{m'A}-x_{mB})}\mathrm{e}^{i\varphi(k_x,p_n)}(\phi^n_{mB})^*\phi^{n'}_{m'A}\langle mB|\, H\, |m'A\rangle \\
= \frac{i}{2\hbar}\sum_{m=1}^{N} & 2it'_4(c+d)\sin[k_x(c+d)](\phi^n_{mA})^*(\phi^{n'}_{m-1A} + \phi^{n'}_{m+1A}) - \mathrm{e}^{i[\varphi(k_x,p_n)-\varphi(k_x,p_{n'})]} \\
& \times 2it'_4(c+d)\sin[k_x(c+d)](\phi^n_{mB})^*(\phi^{n'}_{m-1B} + \phi^{n'}_{m+1B}) - \mathrm{e}^{-i\varphi(k_x,p_{n'})} \\
& \times \{[t'_3(2c+d)\mathrm{e}^{ik_x(2c+d)} - t'_1 d e^{-ik_x d}](\phi^n_{mA})^*(\phi^{n'}_{m-1B} + \phi^{n'}_{m+1B}) + [ct'_2\mathrm{e}^{ik_x c} - (2d+c)t'_5\mathrm{e}^{-ik_x(2d+c)}](\phi^n_{mA})^*\phi^{n'}_{mB}\} \\
& + \mathrm{e}^{i\varphi(k_x,p_n)}\{[t'_1 d e^{ik_x d} - t'_3(2c+d)\mathrm{e}^{-ik_x(2c+d)}](\phi^n_{mB})^*(\phi^{n'}_{m-1A} + \phi^{n'}_{m+1A}) + [(2d+c)t'_5\mathrm{e}^{ik_x(2d+c)} - ct'_2\mathrm{e}^{-ik_x c}](\phi^n_{mB})^*\phi^{n'}_{mA}\},
\end{aligned} \tag{A3}$$

In the absence of external electric field or impurities, substituting the wavefunction $\phi^n_{m\mathrm{A}} = \phi^n_{m\mathrm{B}} = \sqrt{2/(N+1)}\sin\left(\frac{n\pi}{N+1}m\right)$ and the relation $\sin(x) + \sin(y) = 2\sin[(x+y)/2]\cos[(x-y)/2]$ into the above equation, the optical transition matrix elements are obtained as

$$v_{n,n'}(k_x) = \frac{i}{2\hbar}\sum_{m=1}^{N}\{\ 4t_4' i(c+d)\sin[k_x(c+d)]\cos(n'\theta)(\phi_{m\mathrm{A}}^{n})^{*}\phi_{m\mathrm{A}}^{n'} - 4t_4' i(c+d)\sin[k_x(c+d)]\mathrm{e}^{\mathrm{i}[\varphi(k_x,p_n)-\varphi(k_x,p_{n'})]}\cos(n'\theta)(\phi_{m\mathrm{B}}^{n})^{*}$$
$$\times\phi_{m\mathrm{B}}^{n'} - \{2\cos(n'\theta)[t_3'(2c+d)\mathrm{e}^{\mathrm{i}k_x(2c+d)} - t_1' d\mathrm{e}^{-\mathrm{i}k_x d}] + [ct_2'\mathrm{e}^{\mathrm{i}k_x c} - (2d+c)t_5'\mathrm{e}^{-\mathrm{i}k_x(2d+c)}]\}\mathrm{e}^{-\mathrm{i}\varphi(k_x,p_{n'})}(\phi_{m\mathrm{A}}^{n})^{*}\phi_{m\mathrm{B}}^{n'}$$
$$+\{2\cos(n'\theta)[t_1' d\mathrm{e}^{\mathrm{i}k_x d} - t_3'(2c+d)\mathrm{e}^{-\mathrm{i}k_x(2c+d)}] + [(2d+c)t_5'\mathrm{e}^{\mathrm{i}k_x(2d+c)} - ct_2'\mathrm{e}^{-\mathrm{i}k_x c}]\}\mathrm{e}^{\mathrm{i}\varphi(k_x,p_n)}(\phi_{m\mathrm{B}}^{n})^{*}\phi_{m\mathrm{A}}^{n'}\}$$
$$= \frac{i}{2\hbar}\sum_{m=1}^{N}[G_{n,n'}(1-\mathrm{e}^{\mathrm{i}[\varphi(k_x,p_n)-\varphi(k_x,p_{n'})]}) + F_{n,n'}\mathrm{e}^{-\mathrm{i}\varphi(k_x,p_{n'})} + F_{n,n'}^{*}\mathrm{e}^{\mathrm{i}\varphi(k_x,p_n)}]K_{n,n'} \tag{A4}$$

where $G_{n,n'} = 4it_4'\cos(n'\theta)(c+d)\sin[k_x(c+d)]$, $F_{n,n'} = 2\cos(n'\theta)[t_1' d\mathrm{e}^{-\mathrm{i}k_x d} - t_3'(2c+d)\mathrm{e}^{\mathrm{i}k_x(2c+d)}] + [(2d+c)t_5'\mathrm{e}^{-\mathrm{i}k_x(2d+c)} - ct_2'\mathrm{e}^{\mathrm{i}k_x c}]$ and the overlap integration $K_{n,n'}$ between A and B atoms corresponding to different subband index is given by

$$K_{n,n'} = \sum_{m=1}^{N}\phi_{m\mathrm{A}}^{n}\phi_{m\mathrm{B}}^{n'} = \delta_{n,n'}. \tag{A5}$$

From equation (A5), we can find explicitly that the optical transitions obey the rules $n = n'$ because of the orthogonality of wave functions. However, in presence of the external field, the wavefunctions $\phi_{m\mathrm{A}}^{n}$ and $\phi_{m\mathrm{B}}^{n}$ are no longer the simple sine function and the orthogonality relation in equation (A5) will break down, which means that the optical transitions among all subbands are allowed.

ORCID iDs

Xiaoying Zhou https://orcid.org/0000-0003-0230-1715
Benliang Zhou https://orcid.org/0000-0002-8229-1723
Guanghui Zhou https://orcid.org/0000-0002-1536-3440

References

[1] Li L, Yu Y, Ye G, Ge Q, Ou X, Wu H, Feng D, Chen X H and Zhang Y 2014 *Nat. Nanotech.* **9** 372
[2] Han L, Neal A T, Zhu Z, Luo Z, Xu X, Tománek D and Ye P D 2014 *ACS Nano* **8** 4033
[3] Xia F, Wang H and Jia Y 2014 *Nat. Commun.* **5** 4458
[4] Buscema M, Groenendijk D J, Blanter S I, Steele G A, Herre S, van der Zant J and Castellanos-Gomez A 2014 *Nano Lett* **14** 3347
[5] Lu W, Nan H, Hong J, Chen Y, Zhu C, Zheng L, Ma X, Ni Z, Jin C and Zhang Z 2014 *Nano. Res.* **7** 853
[6] Koenig S P, Doganov R A, Schmidt H, Castro Neto A H and Özyilmaz B 2014 *Appl. Phys. Lett.* **104** 103106
[7] Castellanos-Gomez A, Vicarelli L, Prada E, Joshua O IslandNarasimha-Acharya K L, I Blanter S, Groenendijk D J, Buscema M, Steele G A, Alvarez J V, Zandbergen H W, Palacios J J and Herrevan der Zant S J 2014 *2D Mater.* **1** 025001
[8] Castellanos-Gomez A 2015 *J. Phys. Chem. Lett.* **6** 4280
[9] Ling X, Wang H, Huang S, Xia F and Dresselhaus M S 2015 *Proc. Natl Acad. Sci.* **112** 4523
[10] Wang X, Jones A M, Seyler K L, Tran V, Jia Y, Zhao H, Wang H, Yang L, Xu X and Xia F 2015 *Nat. Nanotech.* **10** 517
[11] Rodin A S, Carvalho A and Castro Neto A H 2014 *Phys. Rev. Lett.* **112** 176801
[12] Li L, Kim J, Jin C, Ye G, Qiu D Y, da Jornada F H, Shi Z, Chen L, Zhang Z, Yang F, Watanabe K, Taniguchi T, Ren W, Louie S G, Chen X, Zhang Y and Wang F 2017 *Nat. Nanotech.* **12** 21
[13] Sherman J R T, Abdelwahab I, Chu L, Poh S M, Liu Y, Lu J, Chen W and Loh K P 2018 *Adv. Mater.* **30** 1704619
[14] Zhou X Y, Zhang R, Sun J P, L Zou Y, Zhang D, Lou W K, Cheng F, Zhou G H, Zhai F and Chang K 2015 *Sci. Rep.* **5** 12295
[15] Zhang R, Zhou X Y, Zhang D, Lou W K, Zhai F and Chang K 2015 *2D Mater.* **2** 045012
[16] Zhou X, Lou W-K, Zhang D, Cheng F, Zhou G and Chang K 2017 *Phys. Rev.* B **95** 045408
[17] Zhou X, Lou W-K, Zhai F and Chang K 2015 *Phys. Rev.* B **92** 165405
[18] Low T, Rodin A S, Carvalho A, Jiang Y, Wang H, Xia F and Castro Neto A H 2014 *Phys. Rev.* B **90** 075434
[19] Tran V and Yang L 2014 *Phys. Rev.* B **89** 245407
[20] Zhang R, Wu Z, Li X J and Chang K 2017 *Phys. Rev.* B **95** 125418
[21] Zahra N and Reza A 2016 *Phys. Rev.* B **94** 035437
[22] Carvalho A, Rodin A S and Castro Neto A H 2014 *Europhys. Lett.* **108** 47005
[23] Ezawa M 2014 *New J. Phys.* **16** 115004
[24] Ren Y, Liu P, Zhou B, Zhou X and Zhou G 2019 *Phys. Rev. Applied* **12** 064025
[25] Sisakht E T, Zare M H and Fazileh F 2015 *Phys. Rev.* B **91** 085409
[26] Han X, Stewart H M, Shevlin S A, Catlow C R A and Zheng X G 2014 *Nano Lett.* **14** 4607
[27] Paul M D, Gopinath D, Cupo A, Parkin W M, Liang L, Kharche N, Ling X, Huang S, Dresselhaus M S, Meunier V and Drndić M 2016 *ACS Nano* **10** 5687
[28] Nakanishi Y, Ishi A, Ohata C, Soriano D, Iwaki R, Nomura K, Hasegawa M, Nakamura T, Katsumoto S, Roche S and Haruyama J 2017 *Nano Res* **10** 718
[29] Watts M C, Picco L, Freddie S r P, Cullen P L, Miller t S, Bartu S P, Payton O D, Skipper N t., tileli V and Howard C A 2019 *Nature* **568** 216
[30] Fei R and Yang L 2014 *Nano Lett.* **14** 2884
[31] Guo H, Lu N, Dai J, Wu X and Zeng X C 2014 *J. Phy. Chem.* C **118** 14051
[32] Wei Q and Peng X 2014 *Appl. Phys. Lett.* **104** 251915
[33] de Sousa D J P, de Castro L V, da Costa D R and Milton Pereira J Jr 2016 *Phys. Rev.* B **94** 235415
[34] Liu P, Zhu X, Zhou X, Zhou B, Liao W, Zhou G and Chang K 2019 arXiv:1903.03952
[35] Zhang L and Yuying H 2018 *Sci. Rep.* **8** 6089
[36] Rudenko A N and Katsnelson M I 2014 *Phys. Rev.* B **89** 201408
[37] Rudenko A N, Yuan S and Katsnelson M I 2015 *Phys. Rev.* B **92** 085419
[38] Datta S 2005 *Quantum Transport-Atom to Transistor* (Cambridge: Cambridge University Press)

[39] Taghizadeh Sisakht E, Fazileh F, Zare M H, Zarenia M and Peeters F M 2016 *Phys. Rev.* B **94** 085417
[40] Tang H, Jiang J-W, Wang B-S and Su Z-B 2009 *Sol. State Commun.* **149** 82
[41] Harrison W A 1999 *Elementary Electronic Structure* (Singapore: World Scientific Press)
[42] Ostahie B and Aldea A 2016 *Phys. Rev.* B **93** 075408
[43] Zheng H, Wang Z F, Luo T, Shi Q W and Chen J 2007 *Phys. Rev.* B **75** 165414
[44] Levy N, Burke S A, Meaker K L, Panlasigui M, Zettl A, Guinea F, Castro Neto A H and Crommie M F 2010 *Science* **329** 5991
[45] Naemi Z, Tafreshi M J, Salami N and Shokri A 2019 *J. Mater. Sci.* **54** 7728
[46] Van Hove L 1953 *Phys. Rev.* B **89** 1189
[47] Ando T and Uemura Y 1974 *J. Phys. Soc. Jpn.* **36** 959
[48] Koshino M and Ando T 2008 *Phys. Rev.* B **77** 115313
[49] Nematian H, Moradinasab M, Pourfath M, Fathipour M and Kosina H 2012 *J. Appl. Phys.* **111** 093512
[50] Chung H C, Lee M H, Chang C P and Lin M F 2011 *Opt. Express* **19** 23350
[51] Liu Y, Qiu Z, Carvalho A, Yang B, Xu H, Sherman J R T, Liu W, Antonio H C N, Loh K P and Lu J 2017 *Nano Lett.* **17** 1970
[52] Ghosh B, Singh B, Prasad R and Agarwal A 2016 *Phys. Rev.* B **94** 205426
[53] Zhou B, Zhou B, Liu P and Zhou G 2018 *Physics letters* A **382** 193
[54] Zou Y-L, Song J, Bai C and Chang K 2016 *Phys. Rev.* B **94** 035431
[55] Yu P Y and Cardona M 2010 *Fundamentals of Semiconductors Physics and Materials Properties* 4th edn (Berlin: Springer)